PNAS RESEARCH ARTICLE | PHYSICS

Predicted hot superconductivity in $LaSc_2H_{24}$ under pressure

Xin-Ling He[a,b,c,1], Wenbo Zhao[a,c,1], Yu Xie[a,c], Andreas Hermann[d], Russell J. Hemley[e,f,g], Hanyu Liu[a,c,h,2], and Yanming Ma[a,c,h]

Affiliations are included on p. 5.

Edited by David Ceperley, University of Illinois at Urbana-Champaign, Champaign, IL; received January 27, 2024; accepted May 23, 2024

The recent theory-driven discovery of a class of clathrate hydrides (e.g., CaH_6, YH_6, YH_9, and LaH_{10}) with superconducting critical temperatures (T_c) well above 200 K has opened the prospects for "hot" superconductivity above room temperature under pressure. Recent efforts focus on the search for superconductors among ternary hydrides that accommodate more diverse material types and configurations compared to binary hydrides. Through extensive computational searches, we report the prediction of a unique class of thermodynamically stable clathrate hydrides structures consisting of two previously unreported H_{24} and H_{30} hydrogen clathrate cages at megabar pressures. Among these phases, $LaSc_2H_{24}$ shows potential hot superconductivity at the thermodynamically stable pressure range of 167 to 300 GPa, with calculated T_cs up to 331 K at 250 GPa and 316 K at 167 GPa when the important effects of anharmonicity are included. The very high critical temperatures are attributed to an unusually large hydrogen-derived density of states at the Fermi level arising from the newly reported peculiar H_{30} as well as H_{24} cages in the structure. Our predicted introduction of Sc in the La–H system is expected to facilitate future design and realization of hot superconductors in ternary clathrate superhydrides.

superconductivity | high pressure | hydride

Significance

Room-temperature superconductivity has been a long-held dream of condensed matter physics for over a century. Here, we predict a class of thermodynamically stable clathrate hydrides consisting of two previously unreported H_{24} and H_{30} cages at megabar pressures. Among these hydrides, $LaSc_2H_{24}$ is calculated to exhibit superconductivity with T_c up to 316 K at 167 GPa even when considering the effects of anharmonicity. Such "hot" superconductivity above room temperature is attributed to an unusually large hydrogen-derived density of states at the Fermi level arising from the unusual combination of H_{30} and H_{24} cages of this structure. Further exploration of the La–Sc–H ternary system is expected to facilitate the creation of other high-temperature superconductors.

The quest for materials that superconduct at and even above room temperature remains one of the most important research topics in condensed matter and materials physics. The discovery of covalent H_3S (T_c = 203 K at 155 GPa) (1, 2) and a class of clathrate binary hydrides with high-T_c values in the range of 215 to 260 K at high pressures, including CaH_6 (3, 4), YH_6 (5, 6), YH_9 (6, 7), and LaH_{10} (8–10), all of which inspired by theoretical predictions assuming conventional superconductivity (11–15), has sparked great interest to search for room-temperature superconductivity among compressed hydrides. The first of these theoretically proposed superconducting clathrate hydrides CaH_6 (a predicted T_c of 220 to 235 K at 150 GPa) consisting of sodalite H_{24} cages (13) was recently confirmed experimentally in two independent studies (3, 4). These exciting findings have encouraged the search for other superconducting hydrides with even higher critical temperatures among clathrate-like hydrogen structures.

Recently, attention has been focused on ternary hydrides, since they provide much wider range of candidate compositions and structures that may exhibit high-temperature superconductivity (16–19). For example, our predicted metastable clathrate hydride Li_2MgH_{16} with the highest T_c calculated to date (~473 to 351 K at 250 to 300 GPa) (20) was designed through a strategy of introducing additional electrons from the Li guest metal into the host H_2-based MgH_{16} (21). More recently, guided by theoretical predictions (22–24), the first stoichiometric high-T_c ternary $LaBeH_8$ hydride superconductor with a well-defined crystal structure was synthesized with a measured T_c of 110 K at 80 GPa (25). Previous studies have also reported a series of nonstoichiometric high-T_c ternary alloy hydrides, where the random occupation of metal atoms in the lattice sites can render the crystal structure effectively identical to the parent clathrate structure of the binary systems (26–34); these include theoretically predicted $CaYH_{12}$ (258 K at 200 GPa) (26) and YLu_3H_{24} (288 K at 110 GPa) (29), as well as the experimentally synthesized $(La,Y)H_{10}$ (~253 K at 183 GPa) (31) and $(La,Ce)H_9$ (148 to 178 K at 97 to 172 GPa) (32, 33). These findings suggest the prospect of finding superconductors with the T_c exceeding room temperature in ternary hydrides. While ultimately such superconductors need to be stabilized and function at much lower pressures, it remains critical to establish whether any upper T_c limits exist for hydride superconductors. Therefore, searching for thermodynamically stable superconducting ternary hydrides with higher T_c than LaH_{10} (250 to 260 K at ~180 GPa) is a pressing task.

LaH_{10} was the first metal superhydride (XH_n, $n > 6$) to be predicted (14, 15), synthesized (35), and shown experimentally to be a near room-temperature superconductor (8), a result that has now been reproduced in experiments on the end-member and LaH_{10}-based alloys by at least three other groups (9, 10, 31, 34). Additional studies indicated that higher T_c

Author contributions: H.L. designed research; X.-L.H. and W.Z. performed research; X.-L.H., W.Z., Y.X., A.H., R.J.H., H.L., and Y.M. analyzed data; and X.-L.H., W.Z., Y.X., A.H., R.J.H., H.L., and Y.M. wrote the paper.

The authors declare no competing interest.

This article is a PNAS Direct Submission.

[1]X.-L.H. and W.Z. contributed equally to this work.

[2]To whom correspondence may be addressed. Email: hanyuliu@jlu.edu.cn.

This article contains supporting information online at https://www.pnas.org/lookup/suppl/doi:10.1073/pnas.2401840121/-/DCSupplemental.

Published June 20, 2024.

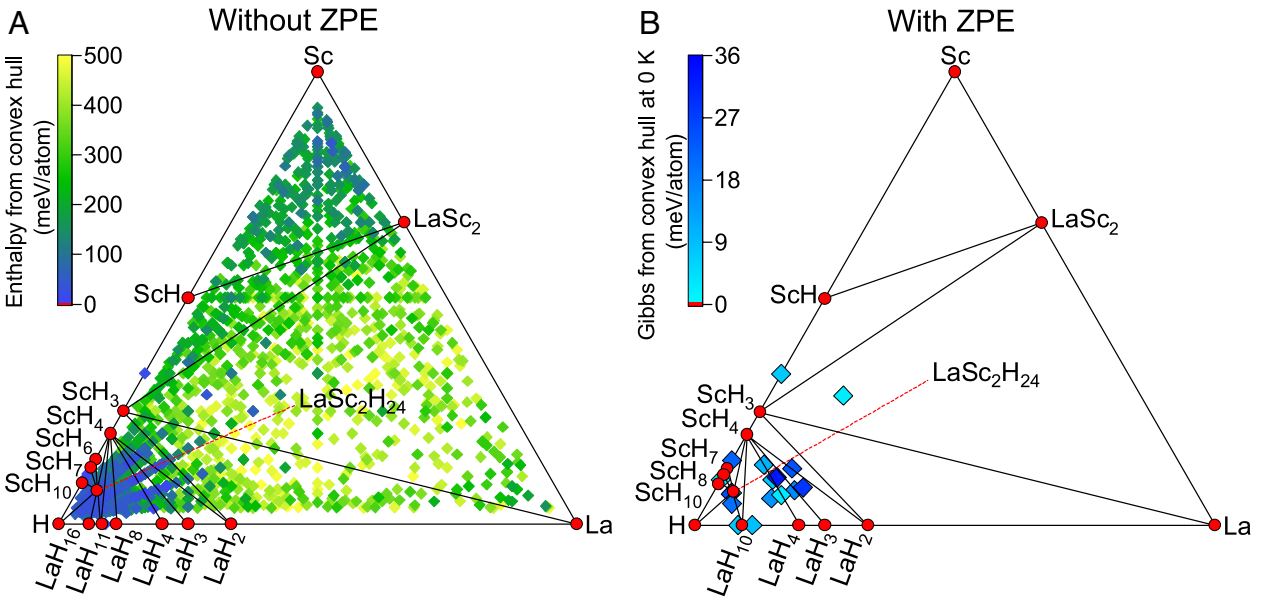

Fig. 1. Calculated ternary phase diagram of the La–Sc–H system relative to elemental La (43–45), Sc (46), and H (39, 40), as well as binary La-H (14, 15, 41), Sc-H (42), and La-Sc at 300 GPa (*A*) without and (*B*) with inclusion of ZPE within the harmonic approximation. Red solid circles and colored squares indicate thermodynamically stable and unstable phases, respectively.

values found for LaH_{10} can arise from different degrees of nitrogen doping (36) and a decrease in T_c can arise with the addition of magnetic impurities (34). It is of great interest to examine the extent to which superconductivity could be further optimized by introducing other elements to form ternary hydrides with higher critical temperatures. An example is a substitutional alloy of $(La,Ce)H_9$ with a higher T_c than pure CeH_9 (32, 33), which is attributed to the element of La having a lower mass than Ce that thereby enhances the Debye temperature of the system. Conversely, note that Sc has a similar valence electronic structure and a lower mass

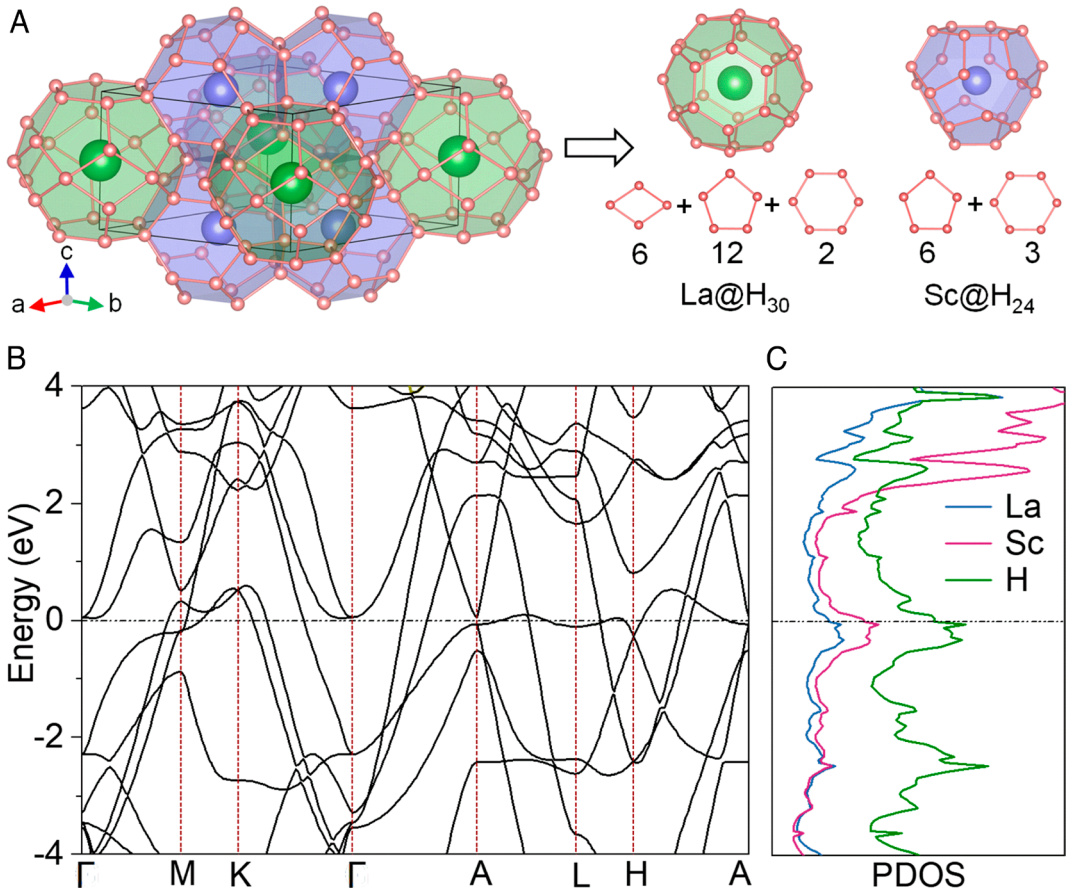

Fig. 2. (*A*) The crystal structure of $LaSc_2H_{24}$ at 300 GPa, consisting of La-centered H_{30} cages and Sc-centered H_{24} cages. Each H_{30} cage contains six rhombuses, 12 pentagons, and two hexagons, while each H_{24} cage consists of six pentagons and three hexagons. (*B*) Electronic band structure and (*C*) PDOS of $LaSc_2H_{24}$ at 300 GPa.

than La, allowing us to expect to tune the superconductivity in the La–H system by the introduction of Sc. To this end, using the swarm-intelligence-based CALYPSO structure prediction method (37, 38) in combination with first-principles calculations, we systematically investigated the crystal structure and superconductivity of the La–Sc–H system under pressure. A remarkable clathrate structure of $LaSc_2H_{24}$ with two unusual H_{24} and H_{30} cages was found and shown to be thermodynamically stable above 167 GPa with considering anharmonic effects. Further electron–phonon coupling (EPC) simulations that include anharmonic effects reveal that the predicted phase is a promising hot superconductor with an estimated T_c of 316 K at 167 GPa (peaking at 331 K at 250 GPa). The results indicate the structure has the lowest stability pressure of any hot superconductor studied to date.

Results and Discussion

Based on the results of variable-composition structure searches, we constructed the ternary phase diagram of the La–Sc–H system at 300 GPa. A unique hydrogen-rich compound with the formula $LaSc_2H_{24}$ and space group *P6/mmm* is identified as thermodynamically stable at 300 GPa (Fig. 1*A* and *SI Appendix*, Fig. S1*A*). As is well known, the contribution of zero-point energy (ZPE) can influence the stability of hydrogen-rich compounds due to the high vibrational frequency associated with the low mass of the H atoms. Including the effect of ZPE, we found that the unique $LaSc_2H_{24}$ compound remains thermodynamically stable at 300 GPa (Fig. 1*B* and *SI Appendix*, Fig. S1*B*). We also investigated the stability of $LaSc_2H_{24}$ at lower pressure by calculating the enthalpy relative to several possible decomposition routes that include the formation of solid hydrogen (39, 40) and binary hydrides (14, 15, 41, 42). Taking into account the effects of both anharmonicity and ZPE, the results indicate that this ternary hydride is thermodynamically stable at pressures as low as 167 GPa (*SI Appendix*, Fig. S2*B*).

Moreover, the ternary $LaSc_2H_{24}$ compound crystallizes in a different superhydride clathrate structure that consists of La-centered H_{30} cages and Sc-centered H_{24} cages with the metal atoms arranged in the AlB_2 structure type (47) (Fig. 2*A*). The H cages themselves have unusual structures, not found in known clathrate (13–15, 19, 20, 48) or zeolite networks (49): six rhombuses, 12 pentagons, and two hexagons comprise each H_{30} cage, while each H_{24} cage consists of six pentagons and three hexagons. Notably, the H–H bond lengths of 1.08, 1.12, 1.16, and 1.20 Å at 300 GPa are slightly longer than the H–H distance (0.98 Å) predicted for monatomic solid hydrogen at 500 GPa (50, 51). On the other hand, these H–H distances are similar to those found in superconducting hydrogen clathrate structures, such as CaH_6 (1.24 Å at 150 GPa) (13) and LaH_{10} (1.07 and 1.16 Å at 300 GPa) (14, 15); the results contrast with the more strongly covalent molecular H–H bond lengths (e.g., <0.8 Å) found in other identified hydrogen-rich compounds that are either low T_c superconductors or even nonmetallic (21, 52, 53), although there are exceptions (54, 55). The H atoms in $LaSc_2H_{24}$ form a weak covalently bonded nonmolecular hydrogen sublattice typical of those found in other clathrate hydride structures and associated with their very high-T_c superconductivity.

Previous studies have established that the size of the metal atom is crucial to the stability of these hydrogen-rich clathrate structures (e.g., refs. 14 and 15). Subsequent investigations of the relationship between the size of the metal atom *M* and the structure of the hydrogenic lattice using the Density Functional Theory (DFT)-Chemical Pressure method also showed that La and Ca atoms comfortably fit the H_{32} cage in MH_{10} and H_{24} cage in MH_6, respectively (56). Since the atomic radii of Sc and Ca are close and the configurations of H clathrate structures in $LaSc_2H_{24}$ are similar to the H_{32} cage in MH_{10} and the H_{24} cage in MH_6, the coordination environment of La and Sc in the H_{30} and H_{24} cages, respectively, of the $LaSc_2H_{24}$ structure is consistent with established systematics.

To examine the electronic properties, we calculated the electronic band structure and projected electronic density of states (PDOS) of $LaSc_2H_{24}$ at 300 GPa. As shown in Fig. 2*B*, several electronic bands cross the Fermi level, indicating the metallic character of $LaSc_2H_{24}$. The PDOS of $LaSc_2H_{24}$ (Fig. 2*C*) also shows a large H-derived DOS (0.11 states/spin/Ry/Å^3) at the Fermi level which is slightly higher than that in LaH_{10} (0.09 states/spin/Ry/Å^3)

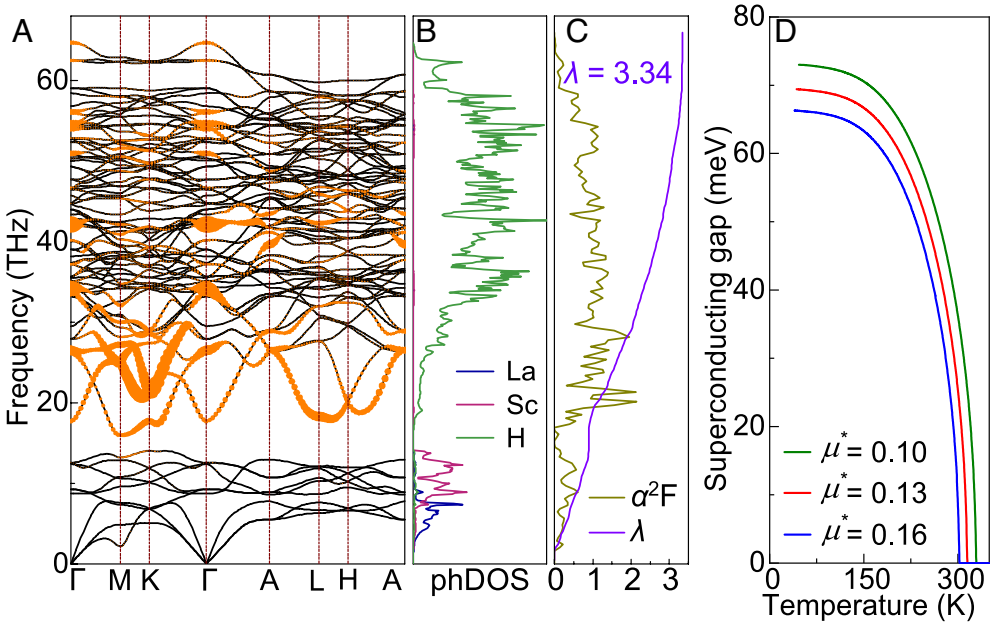

Fig. 3. Lattice dynamics and superconducting properties of $LaSc_2H_{24}$ within the harmonic approximation at 300 GPa. (*A*) Phonon spectra, where orange solid circles show the phonon linewidth with a radius proportional to its strength, (*B*) projected phDOS, (*C*) Eliashberg spectral function $\alpha^2F(\omega)$ as well as the electron–phonon integral $\lambda(\omega)$, and (*D*) superconducting gap.

Table 1. The calculated EPC constant λ, phonon frequency logarithmic average ω_{log} (K), electronic density of states at the Fermi level $N(E_f)$ (states/spin/Ry/f.u.), and superconducting critical temperature T_c (K) with $\mu*$ = 0.16 to 0.1 by numerically solving the isotropic Eliashberg equations for $LaSc_2H_{24}$ within the harmonic and anharmonic approximation at different pressures (GPa).

Calculation	Pressure	λ	ω_{log}	$N(E_f)$	T_c
Harmonic	290	3.56	865	18.69	311 to 339
	300	3.34	968	17.27	303 to 329
	350	2.20	1,294	15.64	266 to 294
Anharmonic	150	3.94	745	18.44	281 to 311
	167	3.73	794	18.76	285 to 316
	200	3.21	965	19.31	291 to 325
	250	2.89	1,075	19.63	296 to 331
	300	2.61	1,165	19.61	293 to 330

at 300 GPa (14, 15), indicating that $LaSc_2H_{24}$ is expected to exhibit H-dominated high-temperature superconductivity. Full phonon and EPC calculations were thus carried out within the harmonic approximation. The phonon dispersion calculations revealed an absence of imaginary frequencies and thus dynamical stability of the structure at 300 GPa (Fig. 3*A*). The phonon density of states (phDOS) shows that the phonons below 16 THz are associated with vibrations of the La and Sc atoms, whereas modes from 16 to 65 THz mainly involve the H atoms (Fig. 3*B*).

The calculated total EPC constant (λ) obtained by integrating over all available phonon frequencies was found to be 3.34 at 300 GPa. The EPC of H modes dominates the contribution to this large λ (i.e., 74%; Fig. 3*C*), especially the soft phonons between 16 and 29 THz, which have a large phonon linewidth (Fig. 3*A*). For strong EPC with $\lambda > 1.5$, direct numerical solution of the Eliashberg equations give an accurate description of the superconducting properties (57, 58). The results reveal a temperature-dependent superconducting energy gap with a predicted T_c of 303 to 329 K at 300 GPa, assuming the Coulomb pseudopotential μ^* of 0.16 to 0.1 (Fig. 3*D*). In addition, our harmonic phonon calculations indicate that $LaSc_2H_{24}$ is dynamically stable down to 290 GPa (*SI Appendix*, Fig. S3*A*), developing a harmonic instability at lower pressures (*SI Appendix*, Fig. S4). We further explored the superconductivity in the 290 to 350 GPa pressure range within the harmonic approximation. As can be seen from Table 1, the λ and T_c of $LaSc_2H_{24}$ decrease with increasing pressure, whereas ω_{log} increases, consistent with hardening on compression of the lower frequency phonons with their large EPC (*SI Appendix*, Fig. S3). Similar results were found for the LaH_{10} and YH_{10} (14, 15).

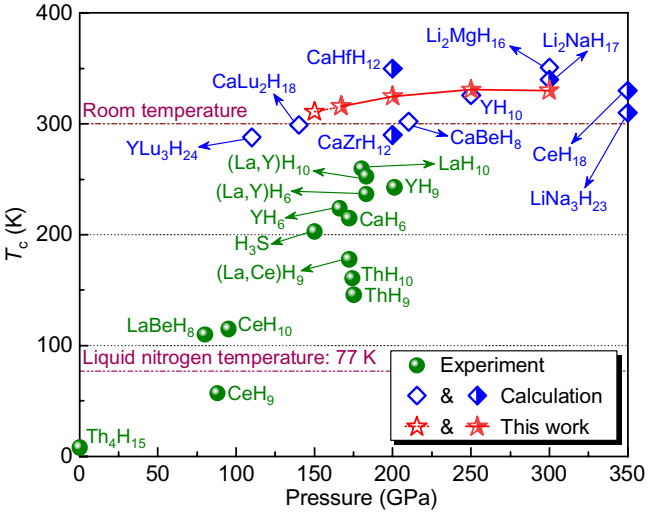

Fig. 4. Pressure dependence of T_c values for typical superconductors. The green filled circles represent the T_c values of well-known superconductors from experiments (1–10, 16–18, 25, 31–33). The blue half-filled (unfilled) rhombuses represent the T_c values of the predicted thermodynamically stable (metastable) hydrides (14, 15, 19, 20, 24, 29, 30, 48). The red half-filled (unfilled) stars mark the T_c values (with μ^* of 0.1) of the thermodynamically stable (metastable) $LaSc_2H_{24}$ by considering anharmonic effects at a pressure range of 150 to 300 GPa.

It is known that anharmonic effects of quantum nuclear and/or thermal origin can affect both the dynamic stability and superconductivity in many compressed hydrides (59–61). We thus performed anharmonic phonon calculations for $LaSc_2H_{24}$ under pressure using the stochastic self-consistent harmonic approximation (SSCHA) approach (59, 62). SSCHA structural relaxation calculations show that anharmonic effects slightly modify the crystal structure of $LaSc_2H_{24}$ (*SI Appendix*, Table S2). For example, the calculated structural parameters and H–H distances at 300 GPa increase slightly by 1.7% and 2.8%, respectively, which induces a change in electronic properties, specifically a higher electronic density of states at the Fermi level $N(E_f)$ (Table 1).

To further explore how anharmonic effects affect the superconductivity, we carried out the SSCHA calculations for lattice phonons of $LaSc_2H_{24}$. The renormalized phonon spectra at the anharmonic level indicate that $LaSc_2H_{24}$ is dynamically stable down to 150 GPa (*SI Appendix*, Fig. S4), which is significantly lower than the harmonic approximation result of 290 GPa. Simulations of the superconductivity that include anharmonicity via renormalized phonon frequencies predict that the critical temperature remains very high, e.g., with T_c = 331 K at 250 GPa ($\mu^*$of 0.1; Table 1). The calculated T_c is larger than that originally calculated for LaH_{10} using similar theoretical techniques (14, 15). Given the close agreement between theory and experiment for the maximum T_c of LaH_{10} [~280 K (14, 15) and 260 K (8–10), respectively, near ~200 GPa], the result indicates the potentially important role of incorporating Sc in the La–H system for realizing superconductivity above room temperature. Moreover, the T_c is predicted to remain very high (316 K with μ^* of 0.1) at a much more accessible pressure of 167 GPa.

Furthermore, we find that the inclusion of self-consistent anharmonic and nuclear quantum effects significantly expands the stability range of the compound, but this has relatively little effect on the calculated T_c (~330 K at 300 GPa). In addition, the ab initio molecular dynamics (AIMD) simulations at 150 GPa and 300 K show that all atoms remained on the *P6/mmm* lattice sites (*SI Appendix*, Fig. S5), which indicates that $LaSc_2H_{24}$ is robust against thermal fluctuations. Finally, with its critical temperature of 316 K at 167 GPa, the $LaSc_2H_{24}$ phase found here is thermodynamically stable at the lowest pressure compared

to superconductors reported to date with a predicted T_c above room temperature (Fig. 4).

Conclusions

The high-pressure phase diagram of the La–Sc–H system examined using the swarm-intelligence-based CALYPSO structure prediction method in combination with first-principles simulations reveals a unique hexagonal and thermodynamically stable $LaSc_2H_{24}$ phase at megabar pressures. The $LaSc_2H_{24}$ structure consists of a unique three-dimensional H clathrate network containing an unusual combination of H_{24} and H_{30} cages. Most strikingly, self-consistent phonon calculations that take into account anharmonic and nuclear quantum effects predict a superconducting T_c well above room temperature in the 167 to 300 GPa pressure range (up to 331 K at 250 GPa). The results expand our perspective on how ternary hydrides offer a platform to engineer phases with a greater diversity of hydrogen frameworks. More than introducing additional elements (e.g., doping) to shift the Fermi level of the parent binary hydride, unique ternary structure types may form with electronic structures that lead to strong EPC and therefore enhanced superconducting properties. Our results further suggest that hot superconducting hydrides with T_cs exceeding 300 K can exist in the experimentally accessible pressure range at 167 GPa and add to the diversity of clathrate hydride structures predicted by theory and confirmed in the laboratory.

Methods

To explore the thermodynamic stability of La–Sc–H compounds, we have utilized the swarm intelligence structure prediction method as implemented in the CALYPSO code (37, 38), conducting variable-composition searches with up to 32 atoms per primitive cell at 300 GPa. For compositions with enthalpies above the convex hull within 50 meV/atom, further fixed composition structural predictions, with system sizes containing up to 2 formula units per simulation cell, were carried out until they reached convergence after generating about 2,000 structures for each stoichiometry.

The following structural optimization and electronic property calculations were performed using DFT within the Perdew–Burke–Ernzerhof parametrization of the generalized gradient approximation (63), as implemented in the Vienna ab initio simulation package code (64). The all-electron projector augmented wave (PAW) method (65) is employed with valence electrons of $5s^25p^65d^16s^2$, $3s^23p^63d^15s^2$, and $1s^1$ for La, Sc, and H, respectively. A plane-wave basis set with an energy cutoff of 850 eV and uniform Γ-centered k-point grids with a resolution of $2\pi \times 0.03$ $Å^{-1}$ were used in the electronic self-consistent calculations. The structures were fully optimized until the maximum energy and force were less than 10^{-8} eV and 1 meV/Å, respectively.

The harmonic phonon frequencies and EPC were calculated by the Quantum-ESPRESSO package within the density functional perturbation theory (66), where the PAW pseudopotentials (67) were used with a kinetic energy cutoff of 90 Ry and a charge density cutoff of 720 Ry. Self-consistent electron density and EPC were calculated by employing 24 × 24 × 24 k-point meshes and 6 × 6 × 6 q-point meshes for $LaSc_2H_{24}$. The anharmonic effects were estimated using the SSCHA code (59, 62). The SSCHA calculations were performed using a 2 × 2 × 2 supercell containing 216 atoms at 0 K, which yielded anharmonic dynamical matrices on a commensurate 2 × 2 × 2 q-point grid.

An 80 Ry energy cutoff and a 3 × 3 × 3 k-point mesh for the Brillouin zone integrations were sufficient in the supercell to converge the SSCHA gradient. The anharmonic phonon frequencies were obtained from the positional free energy Hessian including the third-order terms. Harmonic phonon frequencies and electron–phonon matrix elements were calculated on a grid of 6 × 6 × 6 points. The difference between the harmonic and anharmonic dynamical matrices in the 2 × 2 × 2 phonon-momentum grid was interpolated to a 6 × 6 × 6 grid. Adding the harmonic 6 × 6 × 6 grid dynamical matrices to the result, the anharmonic 6 × 6 × 6 q-grid dynamical matrices were obtained. The ZPE is calculated within the harmonic approximation at 300 GPa. To evaluate the lowest pressure required for the thermodynamic stability of $LaSc_2H_{24}$, we recalculated the ZPE of the ternary hydride and selected decomposition routes at the anharmonic level by using the SSCHA within a pressure range of 150 to 300 GPa. In addition, the superconducting gap and T_c values at the harmonic and anharmonic levels were calculated by numerically solving the isotropic Eliashberg equations (57, 58). The Matsubara frequency cutoff is taken to be about 10 times the highest phonon frequency.

The AIMD simulations were carried out using a 2 × 2 × 3 supercell with 324 atoms for $LaSc_2H_{24}$, with Γ point for k-mesh sampling. A Nosé–Hoover thermostat was adopted to perform the *NVT* simulations with a temperature of 300 K and a pressure of 150 GPa lasting for 20 ps with a time step of 0.5 fs. The statistical information of mean square displacements and atomic trajectories was extracted from the last 15 ps.

Data, Materials, and Software Availability. All study data are included in this article and/or *SI Appendix*.

ACKNOWLEDGMENTS. This work was supported by the National Key Research and Development Program of China (Grant No. 2022YFA1402304), National Natural Science Foundation of China (Grant No. 12074138, 52288102, 52090024, and 12374007), Program for Jilin University Science and Technology Innovative Research Team (2021TD-05), the Program for Jilin University Computational Interdisciplinary Innovative Platform, the Strategic Priority Research Program of Chinese Academy of Sciences (Grant No. XDB33000000), the Royal Society International Exchange Scheme (Grant No. IEC\NSFC\201359), US NSF (DMR-2104881), and the Fundamental Research Funds for the Central Universities and computing facilities at the High-Performance Computing Centre of Jilin University.

Author affiliations: [a]Key Laboratory of Material Simulation Methods and Software of Ministry of Education, College of Physics, Jilin University, Changchun 130012, China; [b]Institute of Physics, Henan Academy of Sciences, Zhengzhou 450046, China; [c]State Key Laboratory of Superhard Materials, College of Physics, Jilin University, Changchun 130012, China; [d]Centre for Science at Extreme Conditions and Scottish Universities Physics Alliance, School of Physics and Astronomy, University of Edinburgh, Edinburgh EH9 3FD, United Kingdom; [e]Department of Physics, University of Illinois Chicago, Chicago, IL 60607; [f]Department of Chemistry, University of Illinois Chicago, Chicago, IL60607; [g]Department of Earth and Environmental Sciences, University of Illinois Chicago, Chicago, IL 60607; and [h]International Center of Future Science, Jilin University, Changchun 130012, China

1. A. P. Drozdov, M. I. Eremets, I. A. Troyan, V. Ksenofontov, S. I. Shylin, Conventional superconductivity at 203 kelvin at high pressures in the sulfur hydride system. *Nature* **525**, 73–76 (2015).
2. M. Einaga *et al.*, Crystal structure of the superconducting phase of sulfur hydride. *Nat. Phys.* **12**, 835–838 (2016).
3. L. Ma *et al.*, High-temperature superconducting phase in clathrate calcium hydride CaH_6 up to 215 K at a pressure of 172 GPa. *Phys. Rev. Lett.* **128**, 167001 (2022).
4. Z. Li *et al.*, Superconductivity above 200 K discovered in superhydrides of calcium. *Nat. Commun.* **13**, 2863 (2022).
5. I. A. Troyan *et al.*, Anomalous high-temperature superconductivity in YH_6. *Adv. Mater.* **33**, 2006832 (2021).
6. P. Kong *et al.*, Superconductivity up to 243 K in the yttrium-hydrogen system under high pressure. *Nat. Commun.* **12**, 5075 (2021).
7. E. Snider *et al.*, Synthesis of yttrium superhydride superconductor with a transition temperature up to 262 K by catalytic hydrogenation at high pressures. *Phys. Rev. Lett.* **126**, 117003 (2021).
8. M. Somayazulu *et al.*, Evidence for superconductivity above 260 K in lanthanum superhydride at megabar pressures. *Phys. Rev. Lett.* **122**, 027001 (2019).
9. A. P. Drozdov *et al.*, Superconductivity at 250 K in lanthanum hydride under high pressures. *Nature* **569**, 528–531 (2019).
10. F. Hong *et al.*, Superconductivity of lanthanum superhydride investigated using the standard four-probe configuration under high pressures. *Chin. Phys. Lett.* **37**, 107401 (2020).
11. Y. Li, J. Hao, H. Liu, Y. Li, Y. Ma, The metallization and superconductivity of dense hydrogen sulfide. *J. Chem. Phys.* **140**, 174712 (2014).
12. D. Duan *et al.*, Pressure-induced metallization of dense $(H_2S)_2H_2$ with high-T_c superconductivity. *Sci. Rep.* **4**, 6968 (2014).
13. H. Wang, J. S. Tse, K. Tanaka, T. Iitaka, Y. Ma, Superconductive sodalite-like clathrate calcium hydride at high pressures. *Proc. Natl. Acad. Sci. U.S.A.* **109**, 6463–6466 (2012).
14. F. Peng *et al.*, Hydrogen clathrate structures in rare earth hydrides at high pressures: Possible route to room-temperature superconductivity. *Phys. Rev. Lett.* **119**, 107001 (2017).
15. H. Liu, I. I. Naumov, R. Hoffmann, N. W. Ashcroft, R. J. Hemley, Potential high-T_c superconducting lanthanum and yttrium hydrides at high pressure. *Proc. Natl. Acad. Sci. USA* **114**, 6990–6995 (2017).
16. J. A. Flores-Livas *et al.*, A perspective on conventional high-temperature superconductors at high pressure: Methods and materials. *Phys. Rep.* **856**, 1–78 (2020).

17. L. Boeri *et al.*, The 2021 room-temperature superconductivity roadmap. *J. Phys.: Condens. Matter* **34**, 183002 (2022).
18. K. P. Hilleke, E. Zurek, Tuning chemical precompression: Theoretical design and crystal chemistry of novel hydrides in the quest for warm and light superconductivity at ambient pressures. *J. Appl. Phys.* **131**, 070901 (2022).
19. D. An *et al.*, Thermodynamically stable room-temperature superconductors in Li-Na hydrides under high pressures. arXiv [Preprint] (2023). https://doi.org/10.48550/arXiv.2303.09805. Accessed 17 March 2023.
20. Y. Sun, J. Lv, Y. Xie, H. Liu, Y. Ma, Route to a superconducting phase above room temperature in electron-doped hydride compounds under high pressure. *Phys. Rev. Lett.* **123**, 097001 (2019).
21. D. C. Lonie, J. Hooper, B. Altintas, E. Zurek, Metallization of magnesium polyhydrides under pressure. *Phys. Rev. B* **87**, 054107 (2013).
22. S. Di Cataldo, C. Heil, W. von der Linden, L. Boeri, $LaBH_8$: Towards high-T_c low-pressure superconductivity in ternary superhydrides. *Phys. Rev. B* **104**, L020511 (2021).
23. X. Liang *et al.*, Prediction of high-T_c superconductivity in ternary lanthanum borohydrides. *Phys. Rev. B* **104**, 134501 (2021).
24. Z. Zhang *et al.*, Design principles for high-temperature superconductors with a hydrogen-based alloy backbone at moderate pressure. *Phys. Rev. Lett.* **128**, 047001 (2022).
25. Y. Song *et al.*, Stoichiometric ternary superhydride $LaBeH_8$ as a new template for high-temperature superconductivity at 110 K under 80 GPa. *Phys. Rev. Lett.* **130**, 266001 (2023).
26. X. Liang *et al.*, Potential high-T_c superconductivity in $CaYH_{12}$ under pressure. *Phys. Rev. B* **99**, 100505(R) (2019).
27. W. Sukmas, P. Tsuppayakorn-aek, U. Pinsook, T. Bovornratanaraks, Near-room-temperature superconductivity of Mg/Ca substituted metal hexahydride under pressure. *J. Alloys Compd.* **849**, 156434 (2020).
28. P. Song, Z. Hou, K. Nakano, K. Hongo, R. Maezono, Potential high-T_c superconductivity in $YCeH_x$ and $LaCeH_x$ under pressure. *Mater. Today Phys.* **28**, 100873 (2022).
29. M. Du, H. Song, Z. Zhang, D. Duan, T. Cui, Room-temperature superconductivity in Yb/Lu substituted clathrate hexahydrides under moderate pressure. *Research* **2022**, 9784309 (2022).
30. L. Liu *et al.*, Generic rules for achieving room-temperature superconductivity in ternary hydrides with clathrate structures. *Phys. Rev. B* **107**, L020504 (2023).
31. D. V. Semenok *et al.*, Superconductivity at 253 K in lanthanum-yttrium ternary hydrides. *Mater. Today* **48**, 18–28 (2021).
32. J. Bi *et al.*, Giant enhancement of superconducting critical temperature in substitutional alloy $(La, Ce)H_9$. *Nat. Commun.* **13**, 5952 (2022).
33. W. Chen *et al.*, Enhancement of superconducting properties in the La-Ce-H system at moderate pressures. *Nat. Commun.* **14**, 2660 (2023).
34. D. V. Semenok *et al.*, Effect of magnetic impurities on superconductivity in LaH_{10}. *Adv. Mater.* **34**, 2204038 (2022).
35. Z. M. Geballe *et al.*, Synthesis and stability of lanthanum superhydrides. *Angew. Chem. Int. Ed. Engl.* **130**, 696–700 (2018).
36. Y. Ge, F. Zhang, R. J. Hemley, Room-temperature superconductivity in boron- and nitrogen-doped lanthanum superhydride. *Phys. Rev. B* **104**, 214505 (2021).
37. Y. Wang, J. Lv, L. Zhu, Y. Ma, Crystal structure prediction via particle-swarm optimization. *Phys. Rev. B* **82**, 094116 (2010).
38. Y. Wang, J. Lv, L. Zhu, Y. Ma, CALYPSO: A method for crystal structure prediction. *Comput. Phys. Commun.* **183**, 2063–2070 (2012).
39. C. J. Pickard, R. J. Needs, Structure of phase III of solid hydrogen. *Nat. Phys.* **3**, 473–476 (2007).
40. H. Liu, H. Wang, Y. Ma, Quasi-molecular and atomic phases of dense solid hydrogen. *J. Phys. Chem. C* **116**, 9221–9226 (2012).
41. I. A. Kruglov *et al.*, Superconductivity of LaH_{10} and LaH_{16} polyhydrides. *Phys. Rev. B* **101**, 024508 (2020).
42. X. Ye, N. Zarifi, E. Zurek, R. Hoffmann, N. W. Ashcroft, High hydrides of scandium under pressure: Potential superconductors. *J. Phys. Chem. C* **122**, 6298–6309 (2018).
43. F. Porsch, W. B. Holzapfel, Novel reentrant high pressure phase transtion in lanthanum. *Phys. Rev. Lett.* **70**, 4087–4089 (1993).
44. W. Chen *et al.*, Superconductivity and equation of state of lanthanum at megabar pressures. *Phys. Rev. B* **102**, 134510 (2020).
45. L. Chen *et al.*, Phase transitions and properties of lanthanum under high pressures. *J. Phys.: Condens. Matter* **34**, 204005 (2022).
46. Y. Akahama, H. Fujihisa, H. Kawamura, New helical chain structure for scandium at 240 GPa. *Phys. Rev. Lett.* **94**, 195503 (2005).
47. W. Hofmann, W. Jäniche, Die struktur von aluminiumborid AlB_2. *Z. Phys. Chem.* **31B**, 214–222 (1936).
48. X. Zhong *et al.*, Prediction of above-room-temperature superconductivity in lanthanide/actinide extreme superhydrides. *J. Am. Chem. Soc.* **144**, 13394–13400 (2022).
49. The database of zeolite structures, http://asia.iza-structure.org/IZA-SC/ftc_table.php.
50. V. Labet, P. Gonzalez-Morelos, R. Hoffmann, N. W. Ashcroft, A fresh look at dense hydrogen under pressure. I. An introduction to the problem, and an index probing equalization of H-H distances. *J. Chem. Phys.* **136**, 074501 (2012).
51. J. M. McMahon, D. M. Ceperley, Ground-state structures of atomic metallic hydrogen. *Phys. Rev. Lett.* **106**, 165302 (2011).
52. D. V. Semenok *et al.*, Sr-doped superionic hydrogen glass: Synthesis and properties of SrH_{22}. *Adv. Mater.* **34**, 2200924 (2022).
53. P. Baettig, E. Zurek, Pressure-stabilized sodium polyhydrides: NaH_n ($n > 1$). *Phys. Rev. Lett.* **106**, 237002 (2011).
54. B. Chen *et al.*, Phase stability and superconductivity of lead hydrides at high pressure. *Phys. Rev. B* **103**, 035131 (2021).
55. Z. Liu *et al.*, Emergence of near room-temperature superconductivity in hydrides with H_2 molecular units. *Phys. Rev. B* **109**, L180501 (2024).
56. K. P. Hilleke, E. Zurek, Rational design of superconducting metal hydrides via chemical pressure tuning. *Angew. Chem. Int. Ed. Engl.* **61**, e202207589 (2022).
57. A. Sanna *et al.*, Ab initio eliashberg theory: Making genuine predictions of superconducting features. *J. Phys. Soc. Jpn.* **87**, 041012 (2018).
58. The elk code, which is an all-electron full-potential linearised augmented-plane wave code with many advanced features, https://elk.sourceforge.io/.
59. I. Errea, M. Calandra, F. Mauri, First-principles theory of anharmonicity and the inverse isotope effect in superconducting palladium-hydride compounds. *Phys. Rev. Lett.* **111**, 177002 (2013).
60. I. Errea *et al.*, High-pressure hydrogen sulfide from first principles: A strongly anharmonic phonon-mediated superconductor. *Phys. Rev. Lett.* **114**, 157004 (2015).
61. I. Errea *et al.*, Quantum crystal structure in the 250-kelvin superconducting lanthanum hydride. *Nature* **578**, 66–69 (2020).
62. L. Monacelli *et al.*, The stochastic self-consistent harmonic approximation: Calculating vibrational properties of materials with full quantum and anharmonic effects. *J. Phys.: Condens. Matter* **33**, 363001 (2021).
63. J. P. Perdew, K. Burke, M. Ernzerhof, Generalized gradient approximation made simple. *Phys. Rev. Lett.* **77**, 3865–3868 (1996).
64. G. Kresse, J. Furthmüller, Efficient iterative schemes for ab initio total-energy calculations using a plane-wave basis set. *Phys. Rev. B* **54**, 11169–11186 (1996).
65. P. E. Blöchl, Projector augmented-wave method. *Phys. Rev. B* **50**, 17953–17979 (1994).
66. P. Giannozzi *et al.*, QUANTUM ESPRESSO: A modular and open-source software project for quantum simulations of materials. *J. Phys.: Condens. Matter* **21**, 395502 (2009).
67. G. Prandini, A. Marrazzo, I. E. Castelli, N. Mounet, N. Marzari, Precision and efficiency in solid-state pseudopotential calculations. *npj Comput. Mater.* **4**, 72 (2018).